VOL. 3, NO.12 Dec, 2012 ISSN 2079-8407
Journal of Emerging Trends in Computing and Information Sciences

http://www.cisjournal.org

Performance Investigation of Loop and Helical Carbon Nanotube Antennas

[1] Moretadha J. Kadhom, [2] Jaber S. Aziz, [3] R. S. Fyath
[1] College of Engineering, University of Baghdad, Baghdad, Iraq
[2,3] College of Engineering, Alnahrain University, Baghdad, Iraq
[1] Moretadha1982@yahoo.com, [2] jsaziz53@yahoo.com, [3] rsfyath@yahoo.com

ABSTRACT

This paper introduces new configurations for the carbon nanotube (CNT) antenna, namely loop and helical CNT antennas. The design of these antennas depends on the geometry which consists of one or more CNT elements. To model these antennas, the CNT is replaced by an equivalent solid wire having frequency dependent complex permittivity which reflects that of the CNT material. The developed CNT model can be used easily with commercial electromagnetic software solvers to predict the characteristics of these advanced antennas. The simulation results reveal that CNT antennas exhibit multiband operation and this property is more emphasized when loop or helical configurations are used.

Keywords: *Carbon nanotube antenna, Loop CNT antenna, Helical CNT antenna.*

1. INTRODUCTION

Carbon nanotubes (CNTs) are characterized by unique electrical properties which make them good candidates for different applications in electronics and electrical engineering. The potential to make metallic and semiconducting nanosize wires from the same material pushed the CNTs into the limelight of both basic and applied research. In the last years a lot of researches have been focused on the electromagnetic characterization of CNTs in order to highlight their use to build nanointerconnects and nano-antennas, due to their outstanding electrical and thermal properties [1-4]. In its simplest form, CNT has a single wall and can be viewed as seamless cylinders rolled from a graphene sheet. The manner in which this graphene layer is rolled, leads to a metal or semi-conducting single-wall CNT (SWCNT). Recently, loop and helical CNTs have been fabricated successfully by different research groups to achieve better performance characteristics compared with conventional wire counterparts [5-10].

The electromagnetic properties of CNT dipole antenna have been investigated in the literature using different numerical techniques [11-15]. However, the investigation does not extend to address the radiation characteristics of other CNT antenna configurations such as loop and helical types. This issue is addressed in this work after modeling the CNT as an equivalent solid wire having frequency dependent complex permittivity which reflects that of the CNT material. The developed CNT model is then used easily with CST, as a commercial electromagnetic software solver, to predict the characteristics of these advanced antennas. All the antennas considered in this paper are assumed to be made from metal SWCNT elements and simulated using CST Microwave Studio software package.

2. THEORETICAL FRAMEWORK

The unit of CNT conductivity g (as a hollow tube) is measured in Siemens (S), but the conductivity σ in Maxwell's equations is measured in (S/m). The reason for this difference is the geometry of the CNT which leads to considering it as a longitudinal geometry and the derivation of the CNT conductivity is based on this fact. In contrast, the metal wires are usually assumed to be a bulk and the physical geometry is assumed to be a transverse then the unit of the conductivity appears to be (S/m). To solve this problem, the CNT is considered here as having an equivalent cylinder with the effective parameters in order to manipulate it simply with Maxwell's equations. This modification will encompass single-wall CNT (SWCNT) and multi-wall CNT (MWCNT) antennas and can also be applied to the bundle CNT (BCNT) antenna.

In the low-frequency regime, below optical interband transitions ($\omega < (v_F/r)$), where v_F is the Fermi velocity and r is the radius of the CNT, the conductivity of armchair or zigzag SWCNT is given by [16]

$$g(\omega) = -j\frac{2e^2 v_F}{\pi^2 \hbar r(\omega - j\nu)} \quad \ldots(1)$$

where e is the electron charge and $\hbar$ is the reduced Planck's constant ($\hbar = 1.05457266 \times 10^{-34}$ J.s), ν is the phenomenological relaxation frequency ($\nu = \tau^{-1} = 6\mathrm{T}/r$), T is temperature in Kelvin, and τ is relaxation time. Further, $v_F = 3\gamma_0 b/2\hbar$, with ($\gamma_0 = 2.7$ eV at low and middle IR frequencies and $b = 0.142$ nm is the interatomic distance in graphene.

The conductivity of a SWCNT model was derived as one dimensional system, where the current is passing on the surface only. Now, assuming a uniform surface current density $\boldsymbol{K}$ for the SWCNT with radius r and line current density $\boldsymbol{I}$ passing through it, then $\boldsymbol{K}$ is defined as

$$\boldsymbol{K} = \frac{\boldsymbol{I}}{2\pi r} \quad \ldots(2)$$

One can model the CNT as a solid cylinder with radius r and line current density $\boldsymbol{I}$ to give the volume current density

$$\boldsymbol{J} = \frac{\boldsymbol{I}}{\pi r^2} \quad \ldots(3)$$

From eqns. 2 and 3, $\boldsymbol{J} = (2/r)\,\boldsymbol{K}$. Applying Ohm's law $\boldsymbol{J} = \sigma \boldsymbol{E}$ to the effective solid cylinder and $\boldsymbol{K} = g\boldsymbol{E}$ to the SWCNT leads to

$$\sigma = \frac{2}{r} g = -j \frac{4e^2 \upsilon_F}{\pi^2 \hbar r^2 (\omega - j\nu)} \quad \ldots(4)$$

where eqn. 1 has been used. Here, the electric field $\boldsymbol{E}$ is assumed to be the same on the surfaces of hollow and solid cylinders and this assumption will give more confidence to this modeling since the electric field and the line current density are assumed constant. Thus, the factor $(2/r)$ may be considered as a transformation factor from the old to the new version.

The concept of the effective conductivity can be generalized to other quantities such as permittivity and permeability which are considered as main parameters in Maxwell's equations. If the relative permeability is assumed to be unity in all types of CNT then the concern is around the permittivity. The effective conductivity of the CNT is generally a complex quantity and can be expressed for SWCNT or MWCNT as

$$\sigma = \sigma_r + j\,\sigma_i \quad \ldots(5)$$

where σ_r and σ_i are, respectively, the real and imaginary parts of the effective conductivity measured by (S/m). Therefore, from Maxwell's equations one can show that the real and imaginary parts of the relative complex permittivity

$$\varepsilon_c = \acute{\varepsilon}_c - j\acute{\varepsilon}_c^{''} \quad \ldots(6)$$

can be expressed as

$$\acute{\varepsilon}_c = \varepsilon_{rel} + \frac{\sigma_i}{\omega \varepsilon_0} \quad \ldots(7a)$$

$$\acute{\varepsilon}_c^{''} = \frac{\sigma_r}{\omega \varepsilon_0} \quad \ldots(7b)$$

Here ε_{rel} is the relative permittivity of the CNT material and ε_0 is the permittivity of the vacuum. If the imaginary part of the effective conductivity is assumed to be zero then the real part of the complex permittivity $\acute{\varepsilon}_c$ is equal to the relative permittivity as in metals such as a copper and gold (low frequency regime).

The Drude model in term of the relative permittivity of the metals can be expressed as [17]

$$\varepsilon_c(\omega) = \varepsilon_{rel} - \frac{\omega_p^2}{\omega(\omega - j\,\nu_{coll})} \quad \ldots(8)$$

where ω_p is the plasma frequency which is in CNT is found to be

$$\omega_p = \frac{2e}{\pi r}\sqrt{\frac{\upsilon_F}{\varepsilon_0 \hbar}} \quad \ldots(9)$$

and ν_{coll} is the collision frequency in metals and assumed as the same as the relaxation frequency ν in CNTs. For the CNT material with $r = 2.71$ nm ($m = n = 40$), the values of $f_p = \omega_p/2\pi$ and ν are found to be 1212 and 0.77 THz, respectively. This means that the CNT will receive the signal of this frequency and beyond as known from the plasma theory. If one assumes a large SWCNT radius with $r =$ 67 nm ($m = n = 1000$), then plasma frequency of a SWCNT material is 48.481 THz which is equivalent to a receiving antenna of length of 3.1 μm.

In conjunction of complex permittivity with plasma frequency, eqns. 7a and b can be rewritten in term of ω_p as

$$\acute{\varepsilon}_c = \varepsilon_{rel} + \frac{{\omega_p}^2}{\omega^2 + \nu^2} \quad \ldots(10a)$$

$$\acute{\varepsilon}_c^{''} = \frac{{\omega_p}^2 \nu}{\omega(\omega^2 + \nu^2)} \quad \ldots(10b)$$

3. LOOP CNT ANTENNAS

Two loop antennas are introduced here, square loop CNT (SLCNT) and circular loop CNT (CLCNT) antennas as shown in Fig. 1. Each type of these two antennas is assumed to have a dual index of $m = n =$ 100 ($r = 6.78$ nm) and T=250^{0}K. Also, all results are compared with those of a SWCNT dipole antenna having the same tube radius and a length equals to the length of the diameter D_0 of SLCNT or CLCNT antenna. The frequency range is set from $1 - 5000$ GHz such that the first resonance frequencies occur obviously.

3.1 Square Loop CNT Antenna

The diameter D_0 of the SLCNT antenna is related to the length of each SWCNT element as $D_0 = L = 2\,\mu$m. The center of the SLCNT antenna is located at the origin and the discrete port is positioned at ($x = 0,\ y = 0,\ z = L/2$) with delta gap length ($d = 2r$).

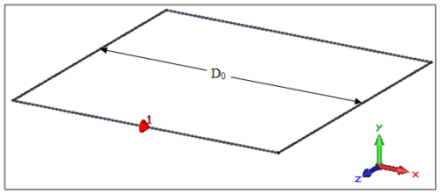

(a)

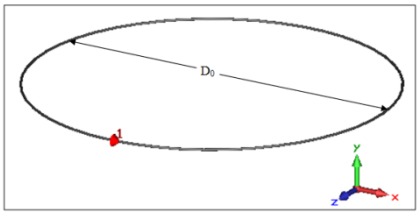

(b)

Fig 1: Geometry representation of (a) SLCNT and (b) CLCNT antennas.

a. S_{11} Parameter

Figure 2 shows the S_{11} parameter of SLCNT and SWCNT dipole antennas. Note that the first resonance frequency of the SLCNT antenna (= 586 GHz) is decreased with respect to the first resonance frequency of the SWCNT dipole antenna (= 850 GHz). At the same time, SLCNT antenna has eight resonance frequencies within the frequency range from 0-3000 GHz while the SWCNT dipole antenna has two resonance frequencies in this range. This makes the SLCNT antenna useful in the field of the multi-band antennas. Also, there is a main feature where the first resonance frequency occurs near to the zero frequency. This makes this antenna be used in the baseband application and this can be satisfied when the input impedance of the discrete port Z_{inp} is set at the counterpart of this frequency.

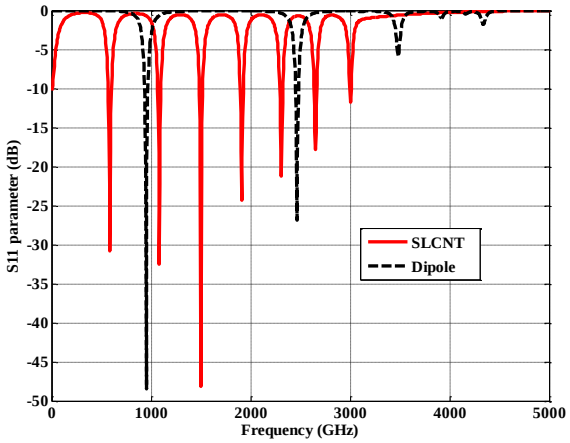

Fig 2: S_{11} parameter of a SLCNT and SWCNT dipole antennas.

b. Input Impedance

Figure 3a and b shows the variation of input resistance and input reactance, respectively, with frequency for the SLCNT and SWCNT dipole antennas. As in the S_{11} parameter, there are eight peaks for both the input resistance and reactance compared with two peaks for the SWCNT dipole antennas within the frequency range (0-3000 GHz). Note that the input resistance and reactance decrease with increasing the resonance frequency for both antennas.

c. Radiation Pattern, Gain, and Efficiency

It is expected that one can modify the directivity in some regions when a SLCNT antenna is used and this is satisfied as shown in Fig. 4. Here a maximum directivity of 2.23 is achieved at 2748 GHz which has a counterpart value equal to 1.57 for the SWCNT dipole antenna. In certain frequency range, the curve of the directivity of the SLCNT antenna seems to have an oscillating behavior on the curve of the SWCNT dipole antenna. This may be considered as a good advantage for investigating various approaches of simulation of CNT antenna since the SLCNT antenna is as a result of a SWCNT dipole antenna, i.e., no complication in geometry is acquired as in the more complex antennas such as a helix.

Figures 5 and 6 show the values of radiation pattern of the SWCNT dipole and SLCNT antennas, respectively. The simulation is carried out at the first resonance frequency for each antenna. The maximum directivity of the SLCNT antenna is 0.419 at $f_{r1} = 586$ GHz compared with 0.248 at $f_{r1} = 851$ GHz for the SWCNT antenna.

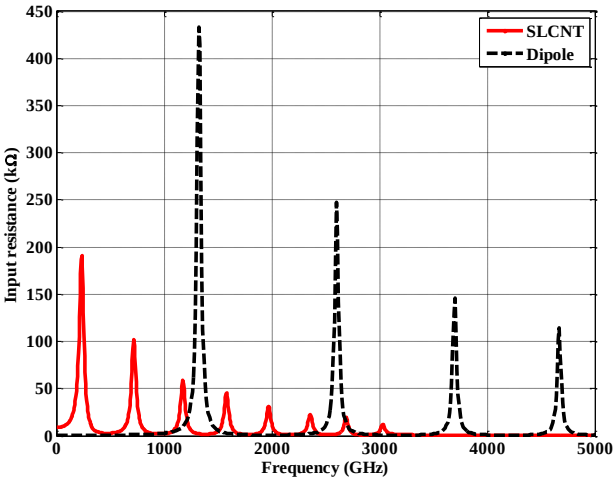

(a)

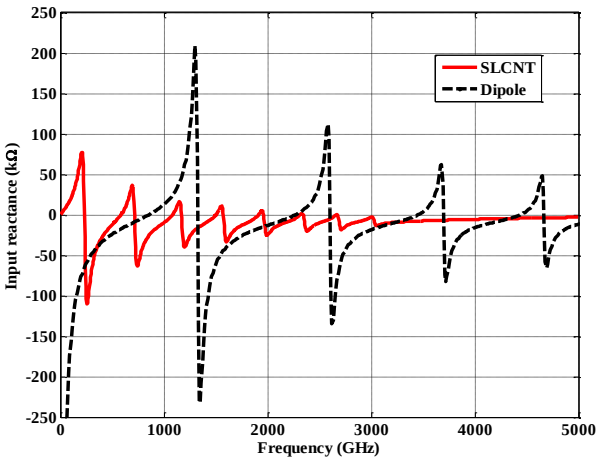

(b)

Fig 3: Input resistance (a) and input reactance (b) of SLCNT and SWCNT dipole antennas.

VOL. 3, NO.12 Dec, 2012 ISSN 2079-8407
Journal of Emerging Trends in Computing and Information Sciences

http://www.cisjournal.org

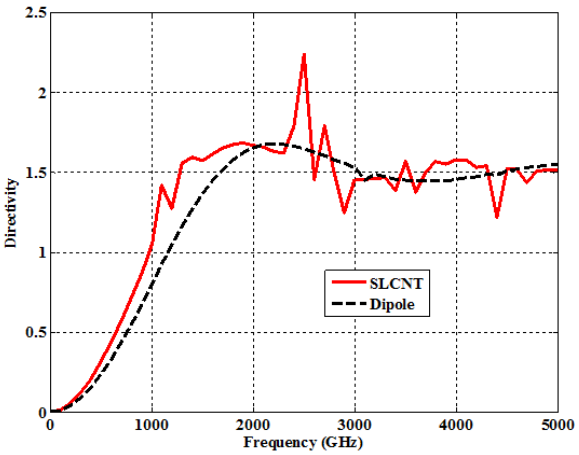

Fig 4: Directivity of SLCNT and SWCNT dipole antennas.

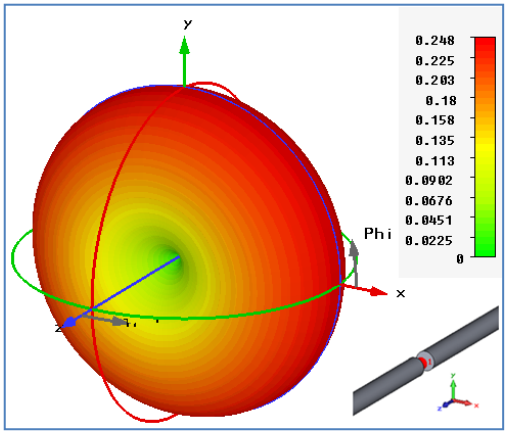

Fig 5: Radiation pattern for SWCNT dipole antenna at $f_{r1} = 851$ GHz.

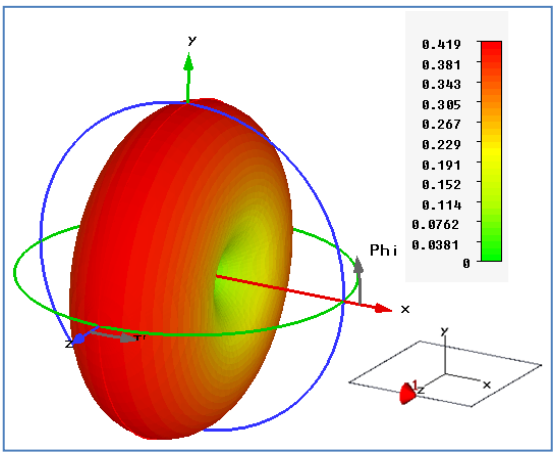

Fig 6: Radiation pattern for SLCNT antenna at $f_{r1} = 586$ GHz.

In addition to the increase in the directivity, SLCNT antenna has an increasing gain as shown in Fig. 7. The total efficiency is modified from 1.3×10^{-5} for the SWCNT dipole antenna to 2.8×10^{-5} for the SLCNT antenna. This change in the total efficiency is due to the small increase in the electrical radius of the SLCNT antenna.

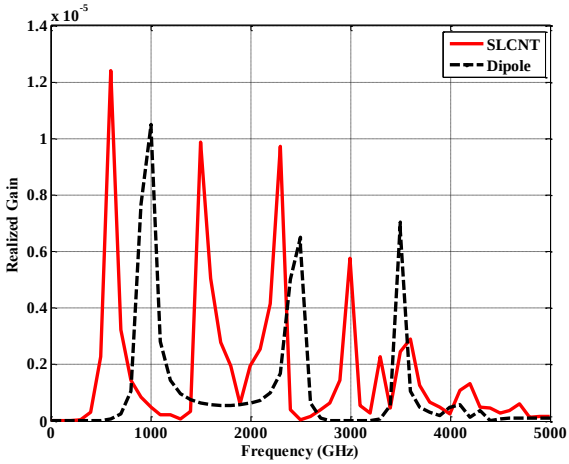

Fig 7: Realized gain of SLCNT and SWCNT dipole antennas.

3.2 Circular Loop CNT Antenna

The circular loop CLCNT antenna seems to have properties more nearly similar to those of the SLCNT antenna as shown in Figs. 8 - 12. Therefore the general comments will be similar to those reported in subsection 3.1.

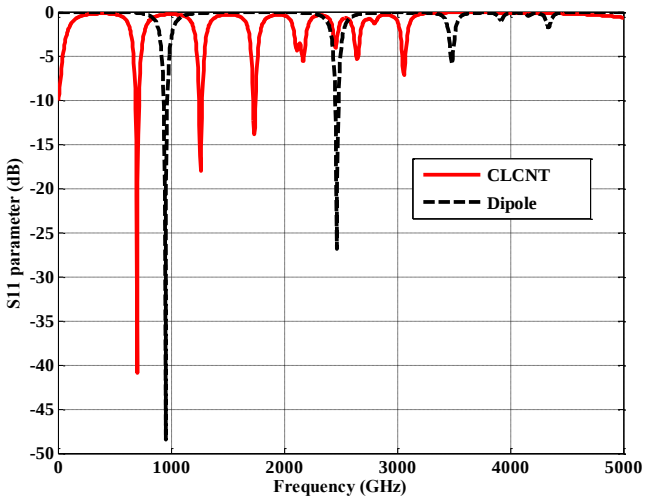

Fig 8: S_{11} parameter of CLCNT and SWCNT dipole antennas.

VOL. 3, NO.12 Dec, 2012 ISSN 2079-8407
Journal of Emerging Trends in Computing and Information Sciences

http://www.cisjournal.org

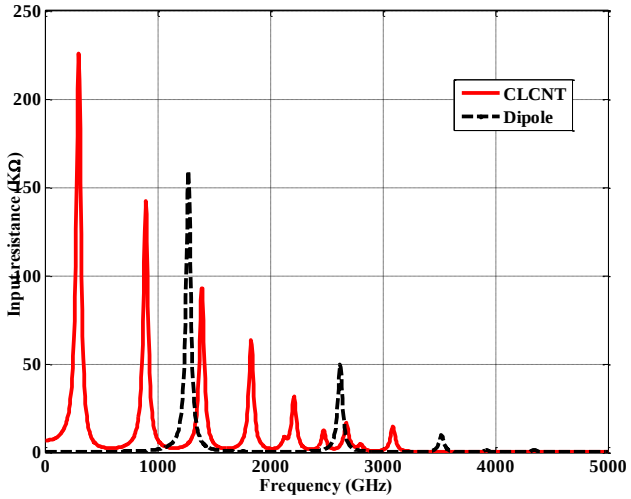

Fig 9: Input resistance of SLCNT and SWCNT dipole antennas.

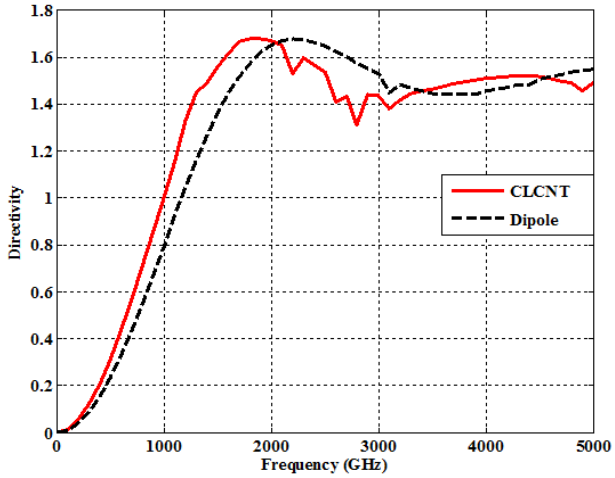

Fig 10: Directivity of CLCNT and SWCNT dipole antennas.

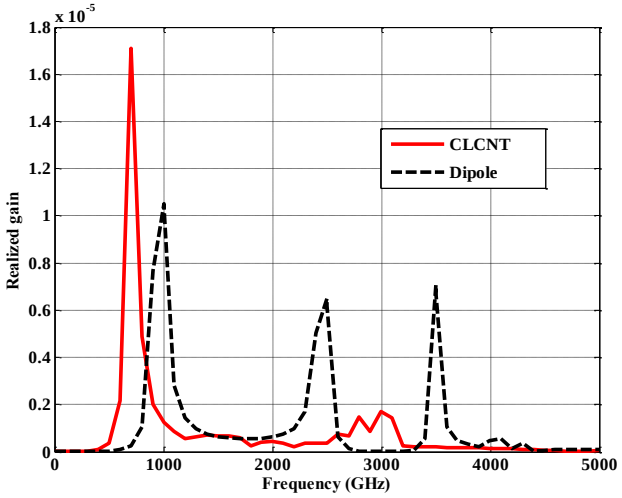

Fig 11: Realized gain of CLCNT and SWCNT dipole antennas.

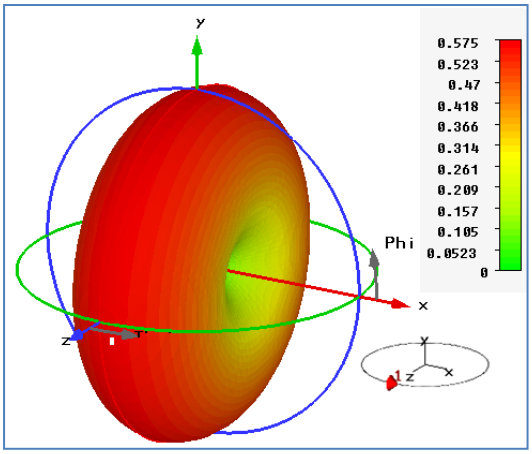

Fig 12: Radiation pattern for CLCNT antenna at $f_r = 703$ GHz.

4. HELICAL SWCNT ANTENNA

In addition to the loop CNT antennas, the helical single-wall carbon nanotube (HSWCNT) antenna is added to the simulated CNT antenna group as shown in Fig. 13. The purpose of this section is to study the properties of this type of antennas and shows the possibility of realization it depending on the constraint that does not affect the physical properties. One of these constraints is the curvature of the CNT which may affect the electrical properties of the helical antenna. In fact, the presence of bending may change the conducting SWCNT into semiconducting SWCNT [18]. Therefore, the ratio of radius of the HSWCNT antenna r_{HSWCNT} to the radius of SWCNT element r is chosen to be large enough.

4.1 Geometry Generation

Initially, the simplest form of a HSWCNT antenna is manipulated. The geometrical configuration of the HSWCNT antenna consists of $N_{HSWCNT} = 4$ turns, diameter $D_0 = 2r_{HSWCNT} = 1\ \mu m$ and spacing $S = 75$ nm between each turn. The total length of the antenna is $H = N_{HSWCNT}S = 0.3\mu m$ while the total length of the SWCNT wire is $L_w = N_{HSWCNT}L_0 = N_{HSWCNT}\sqrt{S^2 + C^2} = 12.57\mu m$ where $L_0 = \sqrt{S^2 + C^2} = 3.143\ \mu m$ is the length of the SWCNT wire between each turn and $C = \pi D_0 = 3.41\ \mu m$ is the circumference of the HSWCNT antenna. The discrete port is located in the middle of the antenna with delta gap distance $d = 4r$ and $n = m = 100$ ($r = 6.78$ nm). CST MWs with the aid of the complex permittivity approach used here to simulate this type of SWCNT antennas. The used constraints are directly related to the CNT materials such as radius and length without going to geometry complexity or discrete port location. The results are compared with a SWCNT antenna with varying length and radius.

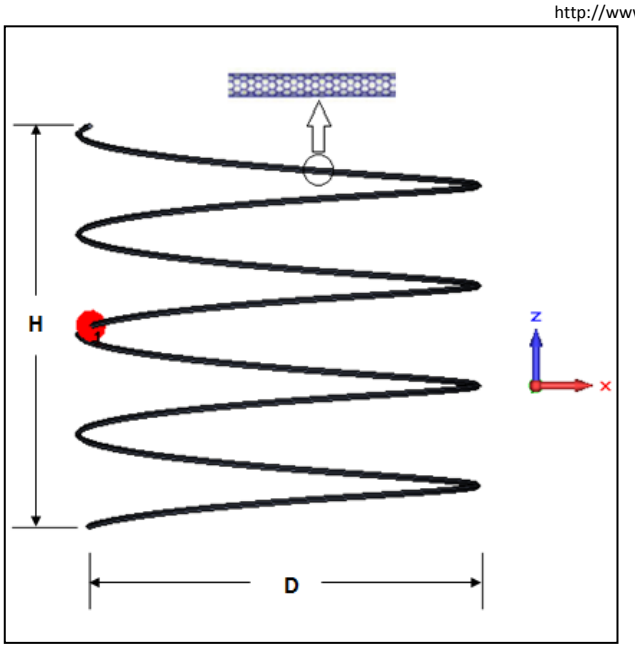

Fig 13: Geometry representation of the HSWCNT antenna.

4.2 S_{11} Characteristics and Resonance Frequencies

Figure 14 shows S_{11} characteristics of the HSWCNT and SWCNT antennas where the length of the SWCNT antenna is chosen to be $L = L_w = 12.57\mu m$. On other side, another SWCNT antenna is simulated but with $L = \mathrm{H} = 1\ \mu m$ for the purpose of finding out which one is close to the HSWCNT antenna. From the values of S_{11} parameter, the input impedance of the discrete port Z_{inp} of each antenna is set by going to the minimum value of S_{11} parameter at first resonance frequency until the convergence is satisfied. The calculated input impedances of the discrete port are $Z_{inp} = 4.439, 11.392,$ and $1.001\ \mathrm{k}\Omega$ for HSWCNT and SWCNT with $L = 12.57$ and $1\ \mu m$ antenna, respectively. The counterparts of the first resonance frequency for the three antennas are computed and found to be $f_r = 226, 161,$ and 1400 GHz.

The first resonance frequency of the HSWCN antenna is very close to the longer SWCNT antenna than to the short SWCNT antenna. This makes the effect of the height H dominant over the length of the SWCNT wire. In addition, the HSWCNT antenna offers a multiple resonance frequencies in the range of 0 -2000 GHz where this antenna can be classified as a multi-band antenna.

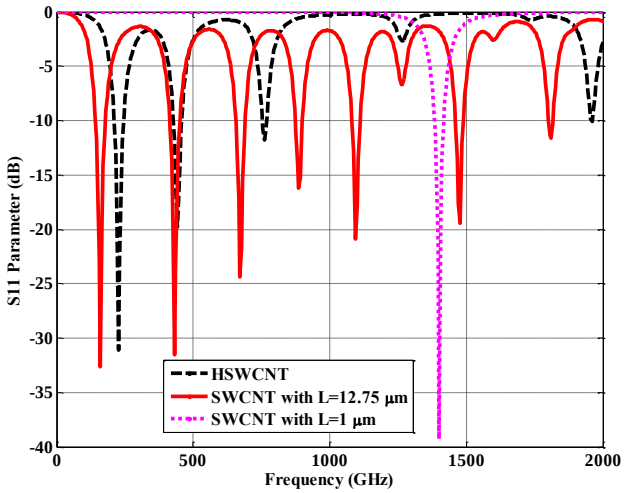

Fig 14: S_{11} parameter of HSWCNT antenna and SWCNT antenna with L=12.57 and 1 μm.

4.3 Directivity and Gain

No effective change in the directivity of the HSWCNT over the directivity of the SWCNT antenna is noticed as shown in Fig. 15. The peak of maximum directivity is about 1.67 for all types.

The key property in the HSWCNT antenna is the modification in the gain as shown in Fig. 16, where for the same wire radius, HSWCNT offers a maximum gain of 0.9×10^{-4} which is considered as a good result with respect to the SWCNT antenna having the same radius. Therefore, the problem of the effective small radius on the antenna gain or efficiency will be solved by changing antenna type to the HSWCNT.

In summary, the HSWCNT antenna has been proposed and simulated in order to solve some problems that are related to the SWCNT antenna. At the same time, the issue of dimensions in nanoarea is very important. This means that, a HSWCNT antenna with $1\mu m$ length will functionalize the role of $12.57\ \mu m$ length with some modification in some properties.

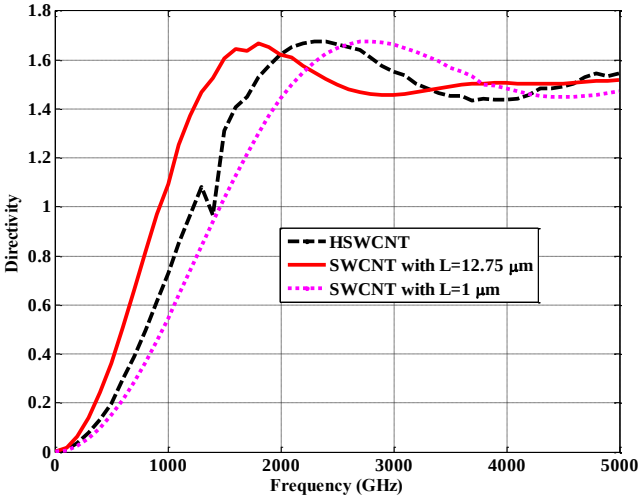

Fig 15: Directivity versus frequency of HSWCNT antenna and SWCNT antenna with $L = 12.57$ and $1\ \mu m$.

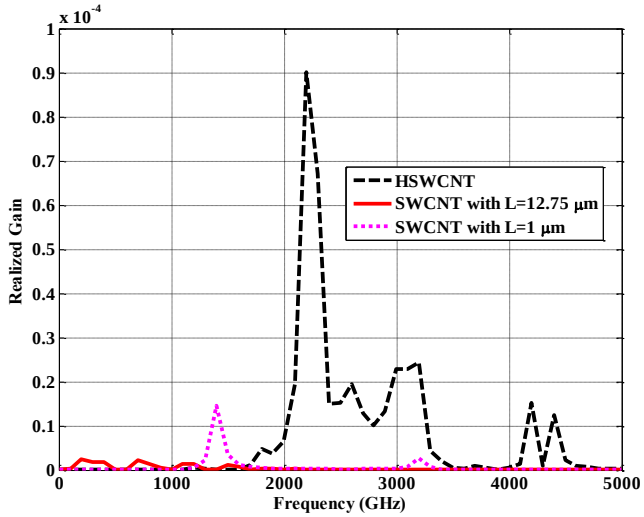

Fig 16: Realized gain versus frequency of HSWCNT antenna and SWCNT antenna with $L = 12.57$ and $1\ \mu m$.

5. CONCLUSIONS

The concept of the effective conductivity of CNT material, which takes into account the frequency dependent complex permittivity, has been adopted as an efficient tool to model various CNT antenna configurations using commercial software package. The simulation results reveal that CNT antennas exhibit multiband operation and this property is more emphasized when loop or helical configurations are used. Further, the helical SWCNT offers one order of magnitude gain enhancement compared with the corresponding SWCNT dipole.

REFERENCES

[1] G. Hanson, "Fundamental Transmitting Properties of Carbon Nanotube Antennas", IEEE Transactions on Antennas and Propagation, Vol. 53, No. 11, PP. 3426-3435, November 2005.

[2] H. Chen, N. Xi, K. Lai, C. Fung, and R. Yang, "Development of Infrared Detectors Using Single Carbon-Nanotube-Based Field-Effect Transistors", IEEE Transactions on Nanotechnology, Vol. 9, No. 5, PP. 582-589, September 2010.

[3] C. Miano, C. Forestiere, A. Maffucci, A. Maksimenko, and G. Slepyan, "Signal Propagation in Carbon Nanotubes of Arbitrary Chirality", IEEE Transactions on Nanotechnology, Vol. 10, No. 1, PP. 135-149, January 2011.

[4] S. Maksimenko, G. Slepyan, A. Nemilentsau, and M. Shuba, "Carbon Nanotube Antenna: Far-Field, Near-Field and Thermal-Noise Properties", Physica E, Vol. 40, PP. 2360–2364, 2008.

[5] D. Fejes and K. Hernádi, "A Review of the Properties and CVD Synthesis of Coiled Carbon Nanotubes", Materials, No. 3, PP. 2618-2642, April, 2010.

[6] P. Bandaru, A. Rao, "Carbon Nanotube Based Coils and Helices", 2010 IEEE Nanotechnology Materials and Devices Conference, PP. 113-118, October, 2010.

[7] F. Sodi, J. Vilatela, J. Rodrı´guez, L. Gutie´rrez , S. Mele´ndez , A. Ra´bago, M. Villarreal, E. Palacios, G. Reiband, M. Terrones, "Carbon Nanotube Bundles Self-assembled in Double Helix Microstructures", Elsevier, Carbon 50, PP. 3688 – 3693, March 2012.

[8] Z. Ghahfarokhi and H. Golestanian, "Effects of Nanotube Helical Angle on Mechanical Properties of Carbon Nanotube Reinforced Polymer Composites", Elsevier, Computational Materials Science 50, PP. 3171-3177, June 2011.

[9] R. Pipesa, P. Hubert, " Helical Carbon Nanotube Arrays: Mechanical Properties", Elsevier, Composites Science and Technology 62, PP. 419-428, 2002.

[10] R. Pipesa, P. Hubert, "Helical Carbon Nanotube Arrays: Thermal Expansion", Elsevier, Composites Science and Technology 63, PP. 1571–1579, 2003.

[11] G. Hanson, "Fundamental Transmitting Properties of Carbon Nanotube Antennas", IEEE Transactions on Antennas and Propagation, Vol. 53, No. 11, PP. 3426-3435, November 2005.

[12] P. Burke, S. Li, and Z. Yu,"Quantitative Theory of Nanowire and Nanotube Antenna Performance", IEEE Transactions on Nanotechnology, Vol. 5, No. 4, PP. 314-334, July 2006.

[13] G. Hanson, "Current on an Infinitely-Long Carbon Nanotube Antenna Excited by a Gap Generator", IEEE Transactions on Antennas and Propagation, Vol. 54, N0. 1, PP. 76-81, January 2006.

[14] J. Hao and G. Hanson, "Infrared and Optical Properties of Carbon Nanotube Dipole Antennas", IEEE Transactions on Nanotechnology, Vol. 5, No. 6, PP. 766-775, November 2006.

[15] N. Fichtner, X. Zhou, and P. Russer, "Investigation of Carbon Nanotube Antennas Using Thin Wire Integral Equations", Advances in Radio Science, Vol. 6, PP. 209–211, 2008.

[16] M. Voutilainen, E. Seppälä, P. Pasanen, and M. Oksanen, "Graphene and Carbon Nanotube Applications in Mobile Devices", IEEE Transactions on Electron Devices, Vol. 59, No. 11, PP. 2876-2887, November 2012.

[17] K. Zhang and D. Li, "Electromagnetic Theory for Microwaves and Optoelectronics", Springer-Verlag Berlin Heidelberg, 2nd edition, New York, 2008.

[18] H. TABAR, "Computational Physics of Carbon Nanotubes", Cambridge University Press, United Kingdom, 2008.